ECS Transactions, 60 (1) 1225-1230 (2014)
10.1149/06001.1225ecst ©The Electrochemical Society

Efficient and Robust Synthesis of Phase-Shifting Masks in Optical Lithography

Wen Lv, Haiqing Wei, and Shiyuan Liu*

State Key Laboratory of Digital Manufacturing Equipment and Technology,
Huazhong University of Science and Technology, Wuhan 430074, China
*Corresponding author: shyliu@mail.hust.edu.cn

Phase-shifting masks (PSMs) are extensively used in semiconductor industry to push the limit of optical lithography. Their synthesis is generally performed via an optimization method under the nominal process condition, and the synthesis process is time-consuming. In this work, we apply a statistical strategy to optimize the average performance with respect to process fluctuations to enhance the robustness of the synthesized PSM pattern, and employ a cascadic multigrid algorithm to improve its computational efficiency. Moreover, we investigate and discuss the impact of the initial pattern on the synthesized result.

1. Introduction

Phase-shifting masks (PSMs) are extensively used as a resolution enhancement technique in semiconductor industry to push the limit of optical lithography (1,2). Compared to conventional masks with only a binary modulation of light intensity, PSMs introduce phase information in the mask transmittance field. It is observed that a suitable modulation of both the phase and the light intensity passing through the mask can be used effectively to compensate for some of the resolution-limiting effects of optical diffraction (3,4). Generally, the synthesis of PSM is performed via an optimization method that aims at synthesizing an input PSM pattern to deliver a desired output pattern on the wafer (5-7). However, the synthesis is generally under the assumption of an ideal imaging system without any process variations, and the synthesis process is time-consuming.

In this work, we employ a statistical strategy to optimize the average wafer performance with respect to process fluctuations to enhance the robustness of the synthesized PSM (8), and apply a cascadic multigrid (CMG) algorithm to improve the computational efficiency. The CMG algorithm (9) synthesizes the PSM hierarchically. It starts from a relatively coarse mask grid and refines it iteratively in stages, so to achieve significant speedup without compromising numerical accuracy over conventional methods that synthesize PSM on a fixed fine grid. Moreover, we investigate and discuss the impact of the initial pattern on the synthesized PSM.

2. Lithography Imaging Model

The lithography imaging process is often decomposed into two parts, namely the optical image formation and the resist development. The optical image $I(\mathbf{r})$ generated by a

partially coherent imaging system can be expressed by a bilinear transform in the spatial domain

$$I(\mathbf{r}) = \iint J(\mathbf{r}_1 - \mathbf{r}_2) H(\mathbf{r} - \mathbf{r}_1) H^{\dagger}(\mathbf{r} - \mathbf{r}_2) M(\mathbf{r}_1) M^{\dagger}(\mathbf{r}_2) \mathrm{d}\mathbf{r}_1 \mathrm{d}\mathbf{r}_2, \quad [1]$$

where $\mathbf{r}$ represents spatial coordinate (x, y), $J(\mathbf{r}_1, \mathbf{r}_2)$ is the mutual intensity function that describes the coherence of the illumination source, $H(\mathbf{r})$ is the point spread function of the optical system, $M(\mathbf{r})$ is the mask transmittance function, and † denotes complex conjugation. In order to simplify the integral operation in Eq. [1], the optical image formation can be approximated as the superposition of several coherent systems by using the analytical circle-sampling technique

$$I(\mathbf{r}) = \sum_{n}^{N} \mu_n \left| \varphi_n(\mathbf{r}) \otimes M(\mathbf{r}) \right|^2. \quad [2]$$

Here, $\varphi_n(\mathbf{r})$ is the n-th analytical kernel with N kernels in total, μ_n is its eigenvalue, and $\otimes$ denotes the 2-D convolution. In particular, the optical kernels $\{\varphi_n(\mathbf{r})\}$ have analytical form; as a result, the grid size of the kernels can be set at any desired value without re-preforming decomposition. Interested readers may refer to Refs. (10,11) for details.

Subsequently, the optical image $I(\mathbf{r})$ goes through the resist development to form the printed image on the wafer. The resist effect is often approximated by a constant threshold resist model using the following Sigmoid function

$$\mathrm{sig}[I(\mathbf{r})] = \frac{1}{1 + \exp\{-a[I(\mathbf{r}) - t]\}} \quad [3]$$

with a being the steepness of the Sigmoid function and t being the threshold of the resist.

We use $Z(\mathbf{r})$ to denote the output pattern on the wafer of the input mask $M(\mathbf{r})$. Combining Eqs. [2] and [3], we formulate the lithography imaging equation as

$$Z(\mathbf{r}) = \mathrm{sig}[I(\mathbf{r})] = \mathrm{sig}\left[\sum_{n}^{N} \mu_n \left| \varphi_n(\mathbf{r}) \otimes M(\mathbf{r}) \right|^2 \right]. \quad [4]$$

3. Formulation of Robust Phase-Shifting Mask Synthesis

Ideally, the output pattern on the wafer is desired to match the input design intent. However, the optical imaging system typically acts as a “low-pass” spatial frequency filter, and cannot deliver the high frequency components of the intended pattern on wafer. So, the objective of PSM synthesis is to synthesize a PSM pattern to pre-compensate the effect of frequency loss so as to deliver a wafer image closer to the desired pattern. Generally, the PSM synthesis is treated as an optimization problem to find a minimum of a cost function as

$$M = \arg\min_{M} \left[G(M) + \kappa R(M) \right]. \quad [5]$$

Here, $G(M)$ is a metric to evaluate the difference between the output pattern of $M(\mathbf{r})$ and the desired pattern, and $R(M)$ is regularization term with the corresponding weight κ to

promote mask manufacturability.

In this work, we take into account two main process variations in optical lithography, namely exposure dose variation and lens-wafer focus variation. In order to synthesize PSMs that are robust to these two process variations, we employ the statistical edge distance error (EDE) (12,13) as the metric $G(M)$ as

$$G(M) = \sum_{p}^{P} \sum_{q}^{Q} \left\{ \alpha(h_p)\beta(t_q) \left[\frac{\delta_x \cdot \delta_y}{L} \cdot \left\| \text{sig}[I(\mathbf{r}; h_p); t_q] - Z^*(\mathbf{r}) \right\|_2^2 \right] \right\}. \quad [6]$$

Here, $Z^*(\mathbf{r})$ is the desired pattern on the wafer, L is the perimeter of the desired pattern contour, δ_x and δ_y are the lengths of the discretization grid along the x and y directions, respectively, $\alpha(\cdot)$ is the density of a prescribed distribution of defocus, $\beta(\cdot)$ is the density of a prescribed distribution of exposure dose, $\{I(\mathbf{r}; h_p)\}$ are the images corresponding to P sampled defocus values $\{h_p\}$, sig$[I(\mathbf{r}; h_p); t_q]$ represents the output pattern of the defocused image $I(\mathbf{r}; h_p)$ on the wafer under the exposure dose level t_q, and $\|\cdot\|_2$ is the L_2 norm.

4. Cascadic Multigrid Algorithm

We employ a cascadic multigrid (CMG) algorithm to solve Eq. [5]. Since the discretized PSM grid is usually square, we use only a parameter δ to describe the space grid size for simplicity, that means $\delta = \delta_x = \delta_y$. For the setup of CMG algorithm, we define a sequence of spaces $\{\Omega_1, \Omega_2, \ldots, \Omega_C\}$ with the corresponding space grid size $\delta_1 > \delta_2 > \ldots > \delta_C$, where Ω_C denotes the finest grid space currently used for discretization of PSM pattern. The pseudo-code of CMG algorithm is described in the following Table I.

TABLE I. Pseudo-Code of the CMG Algorithm.

The Procedure:
Setup: Set C spaces $\{\Omega_1, \Omega_2, \ldots, \Omega_C\}$, and the initial value M_1^0.
For k=1,2,…,C **do**
1: Solve $M_k^* = \arg\min_M \left[G(M) + \kappa R(M) \right]$, subject to : $M \in \Omega_k$ with an initial value M_k^0;
2: Prolong to next space Ω_{k+1}: $M_k^* \rightarrow M_{k+1}^0$;
3: $k \rightarrow k+1$.
End For
Output: M_C^* is the optimal mask.

The CMG algorithm starts PSM synthesis on the coarsest space. Since the coarsest PSM contains much less optimization variables (grids) than the finest PSM on the fine space, it spends much less runtime to find a solution and is more likely to change each variable. From the perspective of signal processing, the coarse PSM can be considered as the low frequency portions of the pattern. The low frequency portions are first optimized, and then further corrected by adding high frequency details on the refined spaces. By contrast, conventional methods perform PSM synthesis directly on the finest space, where it is expensive to change each variable and impossible to separate and treat efficiently the low frequency information content of the pattern. Therefore, the CMG algorithm can achieve a PSM pattern by taking less runtime with better solution performance than the conventional methods.

5. Simulation Results and Discussions

Simulations were performed on a partially coherent imaging system with an annular source illumination (σ_{out}/σ_{in} = 0.4/0.3). The wavelength in the simulations was set at 193 nm, and the numerical aperture was 1.35. The resist effect was approximated by the Sigmoid function with a = 100 and t = 0.6. Since we focus on the alternating PSM (5,7) in the simulations, the numerical value of the PSM matrix $M(\mathbf{r})$ are subject to the ternary values {-1, 0, 1}, and the black, grey, and write regions in all the masks correspond to -1, 0, and 1, respectively. All the simulations were carried out with in-house Matlab codes on a HPZ820 Workstation (2× 2GHz Xeons with 8Cores/16Threads).

Figure 1 compares the performance of the binary mask and the alternating PSM. Figure 1(a) shows a typical 32 nm L/S pattern, consisting of 401×401 pixels with a grid size of 2 nm. It is noted that the optical image Fig. 1(b) of the binary mask is highly distorted from its input pattern Fig. 1(a). In contrast, the optical image Fig. 1(d) of the alternating PSM is less distorted and has higher image intensity. However, although its printed contour on the wafer is close to the desired contour, it encounters considerable large end error and edge error, as shown in Fig. 1(d). Therefore, it is incompetent to simply input the alternating PSM as mask pattern; the PSM pattern need to be further corrected.

Figure 2 depicts the synthesized alternating PSM patterns by using different methods. As expected, the optimized alternating PSM patterns achieve much smaller EDE compared to that simply input the uncorrected alternating PSM as mask pattern. On the other side, it is observed that the synthesized robust alternating PSM patterns Figs. 2(e), (h) and (k), are quite different from Fig. 2(b) that obtained under the nominal process condition, in containing numerous sub-resolution assist features (SRAFs). The reason might be that defocus from the nominal condition results in much worsened image contrast, thus SRAFs tend to be produced in order to enhance the image quality. Furthermore, we compare the exposure-defocus (E-D) trees of the synthesized alternating PSM patterns by setting the EDE to within ±10% of the CD target in Fig. 3. It is expected

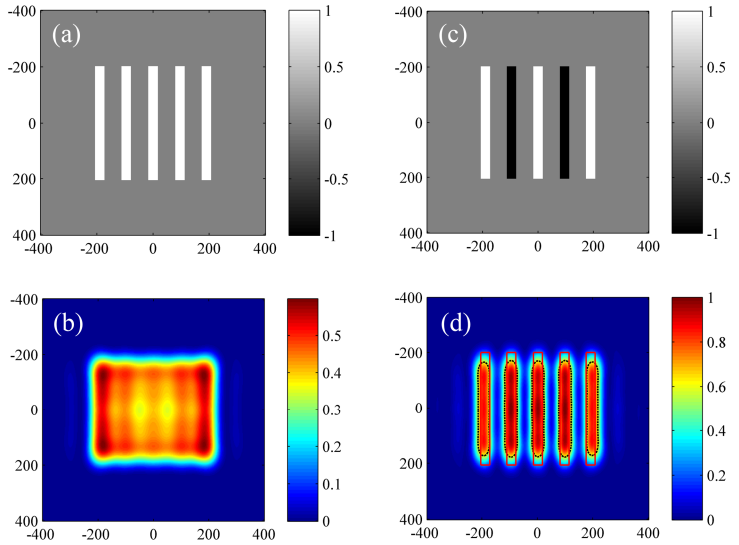

Figure 1. (a) The conventional binary mask, and (b) its optical image on the wafer. (c) The alternating PSM, (d) its optical image on the wafer, the black dashed lines are its resist contour with an EDE of 6.1 nm, and the red solid lines are the desired contour. The horizontal axis and vertical axis denote x position and y position of the patterns in nanometers, respectively.

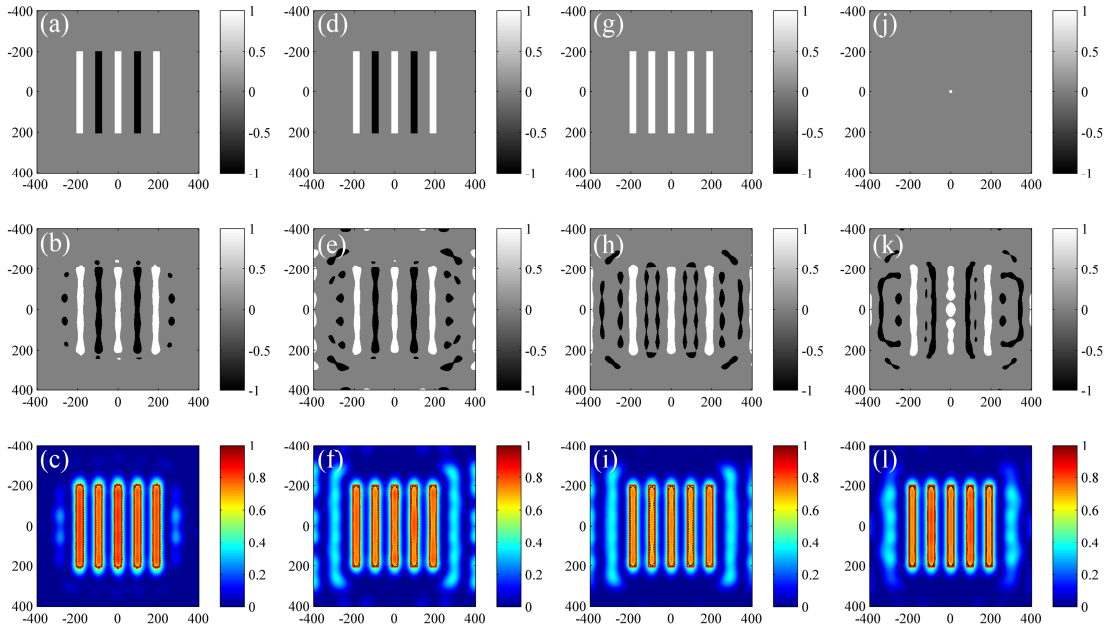

Figure 2. (a) Initial pattern, (b) its synthesized alternating PSM pattern under the nominal process condition, and (c) its optical image on the wafer. (e), (h), and (k) The corresponding synthesized robust alternating PSM patterns with the initial patterns (d), (g), and (j), respectively, and (f), (i) and (l) their corresponding optical image on the wafer. In (c), (f), (i), and (l), the black dashed lines are the corresponding resist contour, and the red solid lines are the desired contour, and their corresponding EDE are 0.7, 1.5, 2.7, and 1.4 nm, respectively. The horizontal axis and vertical axis denote *x* position and *y* position of the patterns in nanometers, respectively.

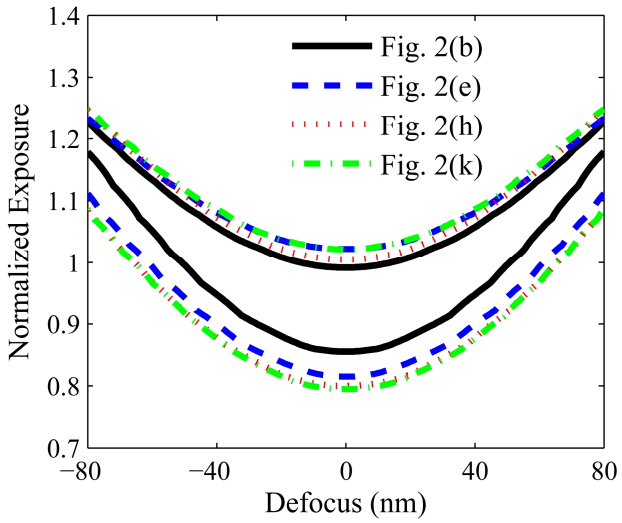

Figure 3. E-D trees of the synthesized mask patterns as shown in Figs. 2(b), 2(e), 2(h) and 2(k).

that the synthesized robust PSM patterns have wider E-D windows. This is because the robust synthesis method further takes the process variations into consideration.

In particular, the synthesized robust alternating PSM patterns differ dramatically with different initial patterns. From Fig. 3, the synthesized alternating PSM as shown in Fig. 2(k) achieves a widest E-D window over the other two. On one hand, these results demonstrate that the PSM synthesis problem is ill-posed and it possesses many local minima. On the other hand, they illustrate that a proper initial pattern can result in a

synthesized mask pattern with better lithographic performance. It indicates that, by setting a proper initial pattern, it can synthesize a better mask pattern that is closer to the true optimal mask pattern.

6. Conclusions

In this work, we formulate the robust PSM synthesis problem in a statistical strategy, and employ a CMG algorithm to solve it. Simulation results show that the synthesized robust PSM patterns possess more SRAFs and have wider E-D windows compared to that obtained under the nominal process condition. Moreover, we investigate the impact of the initial pattern to the synthesized results. It is noted that a proper initial pattern can result in a synthesize mask pattern with better lithographic performance. It is expected that these investigation results will provide a useful way to seek for a better mask pattern that is closer to the true optimal mask pattern.

Acknowledgments

This work was funded by the National Natural Science Foundation of China (Grant No. 91023032, 51005091), the Specialized Research Fund for the Doctoral Program of Higher Education of China (Grant No. 20120142110019), the National Science and Technology Major Project of China (Grant No. 2012ZX02701001), and the National Instrument Development Specific Project of China (Grant No. 2011YQ160002).

References

1. A. K. Wong, *Resolution Enhancement Techniques in Optical Lithography*, SPIE Press, Bellingham, Washington (2001).
2. L. W. Liebmann, S. M. Mansfield, A. K. Wong, M. A. Lavin, W. C. Leipold, and T. G. Dunham, *IBM J. Res. Dev.*, **45**(5), 651 (2001).
3. M. D. Levenson, N. S. Viswanathan, and R. A. Simpson, *IEEE. Trans. Electron Devices,* **ED-29**, 1828 (1982).
4. Y. C. Pati and T. Kailath, *J. Opt. Soc. Am. A*, **11**(9), 2438 (1994).
5. A. Poonawala and P. Milanfar, *Proc. SPIE*, **6154**, 61543H (2006).
6. X. Ma and G. R. Arce, *Opt. Express*, **15**(23), 15066 (2007).
7. S. H. Chan, A. K. Wong, and E. Y. Lam, *Opt. Express*, **16**(19), 14746 (2008).
8. S. Y. Liu, X. J. Zhou, W. Lv, S. Xu, and H. Q. Wei, *Opt. Lett.*, **38**(13), 2168 (2013).
9. W. Lv, E. Y. Lam, H. Q. Wei, and S. Y. Liu, "Cascadic multigrid algorithm for robust inverse mask synthesis in optical lithography," (submitted).
10. P. Gong, S. Y. Liu, W. Lv, and X. J. Zhou, *J. Vac. Sci. Technol. B*, **30**(6), 06FG03 (2012).
11. W. Lv, S. Y. Liu, Q. Xia, X. F. Wu, Y. Shen, and E. Y. Lam, *J. Vac. Sci. Technol. B*, **31**(4), 041605 (2013).
12. W. Lv, Q. Xia, and S. Y. Liu, *Proc. SPIE*, **8683**, 868325 (2013).
13. W. Lv, Q. Xia, and S. Y. Liu, *J. Micro/Nanolith. MEMS MOEMS*, **12**(4), 043003 (2013).